

Optical study of magnetic topological insulator $MnBi_4Te_7$

Zhi-Yu Liao(廖知裕), Bing Shen(沈冰), Xiang-Gang Qiu(邱祥冈), and Bing Xu(许兵)
Citation: Chin. Phys. B, 2024, 33 (**1**): 017802. DOI: 10.1088/1674-1056/ad08aa
Journal homepage: http://cpb.iphy.ac.cn; http://iopscience.iop.org/cpb

What follows is a list of articles you may be interested in

Effect of heating time on structural, morphology, optical, and photocatalytic properties of g-C_3N_4 nanosheets

Nguyen Manh Hung, Le Thi Mai Oanh, Lam Thi Hang, Pham Do Chung, Pham Thi Duyen, Dao Viet Thang, Nguyen Van Minh
Chin. Phys. B, 2020, 29 (**5**): 057801. DOI: 10.1088/1674-1056/ab7e95

Optical investigation of topological semimetal $SrMnSb_2$

Zi-Yang Qiu(邱子阳), Zhi-Yu Liao(廖知裕), Xiang-Gang Qiu(邱祥冈)
Chin. Phys. B, 2019, 28 (**4**): 047801. DOI: 10.1088/1674-1056/28/4/047801

Magnetic field aligned orderly arrangement of Fe_3O_4 nanoparticles in CS/PVA/Fe_3O_4 membranes

Meng Du(杜萌), Xing-Zhong Cao(曹兴忠), Rui Xia(夏锐), Zhong-Po Zhou(周忠坡), Shuo-Xue Jin(靳硕学), Bao-Yi Wang(王宝义)
Chin. Phys. B, 2018, 27 (**2**): 027805. DOI: 10.1088/1674-1056/27/2/027805

Synthesis and microwave absorption properties of graphene-oxide(GO)/polyaniline nanocomposite with gold nanoparticles

Fu Chen (付晨), He Da-Wei (何大伟), WangYong-Sheng (王永生), Fu Ming (富鸣), Geng Xin (耿欣), Zhuo Zu-Liang (卓祖亮)
Chin. Phys. B, 2015, 24 (**8**): 087801. DOI: 10.1088/1674-1056/24/8/087801

Synthesis and microwave absorption properties of graphene-oxide(GO)/polyaniline nanocomposite with Fe_3O_4 particles

Geng Xin (耿欣), He Da-Wei (何大伟), Wang Yong-Sheng (王永生), Zhao Wen (赵文), Zhou Yi-Kang (周亦康), Li Shu-Lei (李树磊)
Chin. Phys. B, 2015, 24 (**2**): 027803. DOI: 10.1088/1674-1056/24/2/027803

RAPID COMMUNICATION

Optical study of magnetic topological insulator $MnBi_4Te_7$

Zhi-Yu Liao(廖知裕)[1,2], Bing Shen(沈冰)[3], Xiang-Gang Qiu(邱祥冈)[1,2,4,†], and Bing Xu(许兵)[1,2,‡]

[1] *Beijing National Laboratory for Condensed Matter Physics, Institute of Physics, Chinese Academy of Sciences, Beijing* 100190, *China*
[2] *School of Physical Sciences, University of Chinese Academy of Sciences, Beijing* 100049, *China*
[3] *State Key Laboratory of Optoelectronic Materials and Technologies, School of Physics, Sun Yat-Sen University, Guangzhou* 510275, *China*
[4] *Songshan Lake Materials Laboratory, Dongguan* 523808, *China*

(Received 7 October 2023; revised manuscript received 1 November 2023; accepted manuscript online 2 November 2023)

We present an infrared spectroscopy study of the magnetic topological insulator $MnBi_4Te_7$ with antiferromagnetic (AFM) order below the Néel temperature $T_N = 13$ K. Our investigation reveals that the low-frequency optical conductivity consists of two Drude peaks, indicating a response of free carriers involving multiple bands. Interestingly, the narrow Drude peak grows strongly as the temperature decreases, while the broad Drude peak remains relatively unchanged. The onset of interband transitions starts around 2000 cm^{-1}, followed by two prominent absorption peaks around 10000 cm^{-1} and 20000 cm^{-1}. Upon cooling, there is a notable transfer of spectral weight from the interband transitions to the Drude response. Below T_N, the AFM transition gives rise to small anomalies of the charge response due to a band reconstruction. These findings provide valuable insights into the interplay between magnetism and the electronic properties in $MnBi_4Te_7$.

Keywords: infrared spectroscopy, magnetic topological insulator, Drude model, band reconstruction

PACS: 78.30.–j, 78.40.Kc, 78.47.–p **DOI:** 10.1088/1674-1056/ad08aa

1. Introduction

Finding various new electronic states and unusual quantum phases has been an important subject in condensed matter physics. Since the nontrivial dissipationless edge state was observed in topological insulators (TIs), significant research efforts have been devoted to introducing magnetism into TIs to form magnetic TIs over the past few years. With the interplay between magnetism and nontrivial band topologies, magnetic TIs can be an ideal materials playground for realization of various peculiar quantum states, such as the quantum anomalous Hall (QAH) state[1–4] and axion insulator.[5–9] In 2013, the QAH effect was realized for the first time in Cr-doped topological $(Bi,Sb)_2Te_3$ film at about 100 mK.[3] Such a low working temperature is due to the inhomogeneous distribution of magnetic dopants. However, stoichiometric topological materials with intrinsic magnetic order can avoid this problem and may be promising systems to find QAH effect at higher temperature.

Recently, the van der Waals layer compound $MnBi_2Te_4$ with antiferromagnetic (AFM) order below $T_N = 24$ K has been proposed to be an intrinsic AFM TI.[10–15] Its rhombohedral crystal structure can be viewed as a stacking of septuple layers along the c axis. Of which one septuple layer contains a magnetic Mn–Te layer inserted into a quintuple layer of topological insulator Bi_2Te_3. Magnetotransport experiments on few-layer flakes of $MnBi_2Te_4$ have revealed signatures of QAH state and axion insulator phase.[16–18] Furthermore, angle-resolved photoemission spectroscopy (ARPES) studies on bulk crystals have observed topological gapless Dirac cone surface states,[19–23] although some research groups have reported gapped Dirac cone surface states.[12,24–26] $MnBi_2Te_4$ can also constitute the progenitor of a modular $(Bi_2Te_3)_n(MnBi_2Te_4)$ series compounds, where the interlayer antiferromagnetic exchange coupling can be weakened by increasing the separation of the magnetic septuple layers with nonmagnetic quintuple layers along the c axis. This offers a new approach to manipulating the band topology. In the case of $MnBi_4Te_7$ with $n = 1$, it exhibits an A-type antiferromagnetic structure, similar to $MnBi_2Te_4$, with in-plane ferromagnetic arrangement coupled antiferromagnetically along the c-axis below $T_N = 13$ K, as revealed by single-crystal neutron diffraction measurement.[27,28] ARPES studies have provided strong evidences of topological surface states on both surface terminations of Bi_2Te_3 and $MnBi_2Te_4$.[13,22,29–36] A gap induced by hybridization effect was identified on the Bi_2Te_3-termination, while a gapless Dirac-cone band structure was observed on the $MnBi_2Te_4$-termination. This suggests different surface magnetic orders on the two terminations and calls for further detailed studies.[34] Meanwhile, the influence of bulk magnetic order on the low-energy excitations is still not fully understood.

In this study, we investigate the bulk electronic properties of $MnBi_4Te_7$ both above and below T_N using infrared spectroscopy. Our optical results reveal the presence of two

†Corresponding author. E-mail: xgqiu@iphy.ac.cn
‡Corresponding author. E-mail: bingxu@iphy.ac.cn

© 2024 Chinese Physical Society and IOP Publishing Ltd

Drude peaks in the low-frequency optical conductivity with a free-carrier response of multiple bands. The interband transitions start above 2000 cm^{-1} and the spectral weight analysis supports the transfer of spectral weight from the interband transitions to the Drude response with decreasing temperature. Furthermore, below T_N, we observe anomalies in the low-frequency optical conductivity, which serve as signatures of a band reconstruction induced by the antiferromagnetic order.

2. Experiment

High-quality single crystals of $MnBi_4Te_7$ were synthesized by a flux method.[19] We measured the *ab*-plane frequency-dependent reflectivity $R(\omega)$ of $MnBi_4Te_7$ with fresh surface at a near-normal angle of incidence, using a Bruker 80v Fourier transform infrared (FTIR) spectrometer. An *in situ* gold evaporation technique[37] was used for obtaining the absolute reflectivity of the sample. Data from 30 cm^{-1} to 12000 cm^{-1} were collected at varying temperatures with a commercial ARS-Helitran cryostat. We obtained the real part of the optical conductivity $\sigma_1(\omega)$ through a Kramers–Kronig analysis of $R(\omega)$. A Hagen–Rubens relation $R(\omega) = 1 - A\sqrt{\omega}$ was applied for low-frequency extrapolation. On the high-frequency side, we used the room-temperature data from 4000 cm^{-1} to 50000 cm^{-1} via a commercial ellipsometer (Woollam VASE). Meanwhile, the high-frequency extrapolation was anchored by the ellipsometry data, where we assumed a constant reflectivity up to 110000 cm^{-1} (13.6 eV), followed by a free-electron (ω^{-4}) response.

3. Results and discussion

The temperature (T) dependence of in-plane resistivity $\rho(T)$ for $MnBi_4Te_7$ shows a metallic characteristic with an anomaly around $T_N = 13$ K due to the AFM phase transition, as shown in the upper inset of Fig. 1(a). This is consistent with the previous results.[27,38,39] Figure 1(a) displays the in-plane reflectivity $R(\omega)$ of $MnBi_4Te_7$ at different temperature up to 6000 cm^{-1}. The lower inset shows the spectrum up to 50000 cm^{-1} at 300 K. It shows a typical metallic response: toward zero frequency $R(\omega)$ approaches nearly unity and increases upon cooling. At higher frequency the reflectivity gradually decreases and drops rapidly near 1500 cm^{-1}, forming a plasma edge. This plasma edge shifts to higher frequency toward lower T.

Figure 1(b) shows the corresponding T-dependent spectra of the real part of the complex dielectric function $\varepsilon_1(\omega)$. The negative value of $\varepsilon_1(\omega)$ at low frequency is another hallmark of metallic response. The zero-crossing in $\varepsilon_1(\omega)$ (marked by the horizontal dashed line) corresponds to the screened plasma frequency $\omega_p^{scr} = \omega_p/\sqrt{\varepsilon_\infty}$, where ω_p is the free-carriers plasma frequency and ε_∞ is the high-frequency dielectric constant. The inset shows the detailed T evolution of ω_p^{scr}. With decreasing T, ω_p^{scr} has a remarkable increase from about 1250 cm^{-1} at 300 K to near 1500 cm^{-1} at 20 K. Moreover, there is a small decrease below T_N, indicating that the AFM order has a weak effect on the charge response.

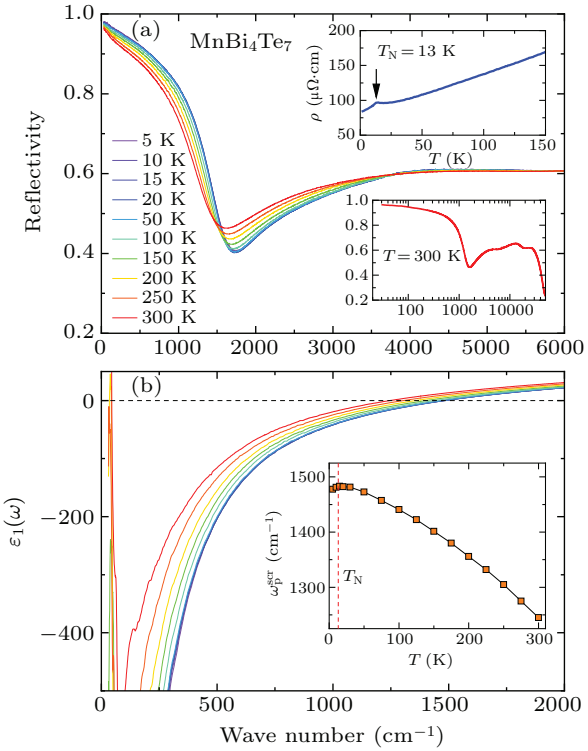


Fig. 1. The measured optical reflectivity and the corresponding real part of the complex dielectric function. (a) T dependence of in-plane reflectivity up to 6000 cm^{-1} for $MnBi_4Te_7$. Insets: T-dependent resistivity (top panel) and reflectivity spectrum up to 50000 cm^{-1} at 300 K (bottom panel). (b) T dependence of the real part of the complex dielectric function $\varepsilon_1(\omega)$. Inset: temperature evolution of the screened plasma frequency extracted from the zero crossing of $\varepsilon_1(\omega)$.

Figure 2(a) displays the T dependence of the real part of the complex optical conductivity $\sigma_1(\omega)$ up to 6000 cm^{-1}. It consists of a narrow Drude peak centered at the origin with a tail extending to about 2000 cm^{-1}. The direct current (dc) conductivity data at 5 K and 300 K (represented by filled circles on the y-axis) obtained from $\rho(T)$ in the upper inset of Fig. 1(a) agree well with the zero-frequency extrapolation of $\sigma_1(\omega)$. Toward higher frequency above 2000 cm^{-1}, $\sigma_1(\omega)$ turns to increase due to the onset of electronic interband transitions. Notably, upon cooling, the Drude peak grows strongly while the onset of region of the interband transitions is suppressed. As shown in the inset, we also compare the full-range spectrum of $\sigma_1(\omega)$ at 300 K between $MnBi_4Te_7$ and the previously reported $MnBi_2Te_4$.[40] The overall feature of the spectrum is very similar for both compounds, consisting of a Drude response at low frequency and two dominant interband transition peaks around 10000 cm^{-1} and 20000 cm^{-1}. Note that the low-frequency of $\sigma_1(\omega)$ for $MnBi_4Te_7$ is higher than that of $MnBi_2Te_4$, indicating a better carrier conduction in the former compound.

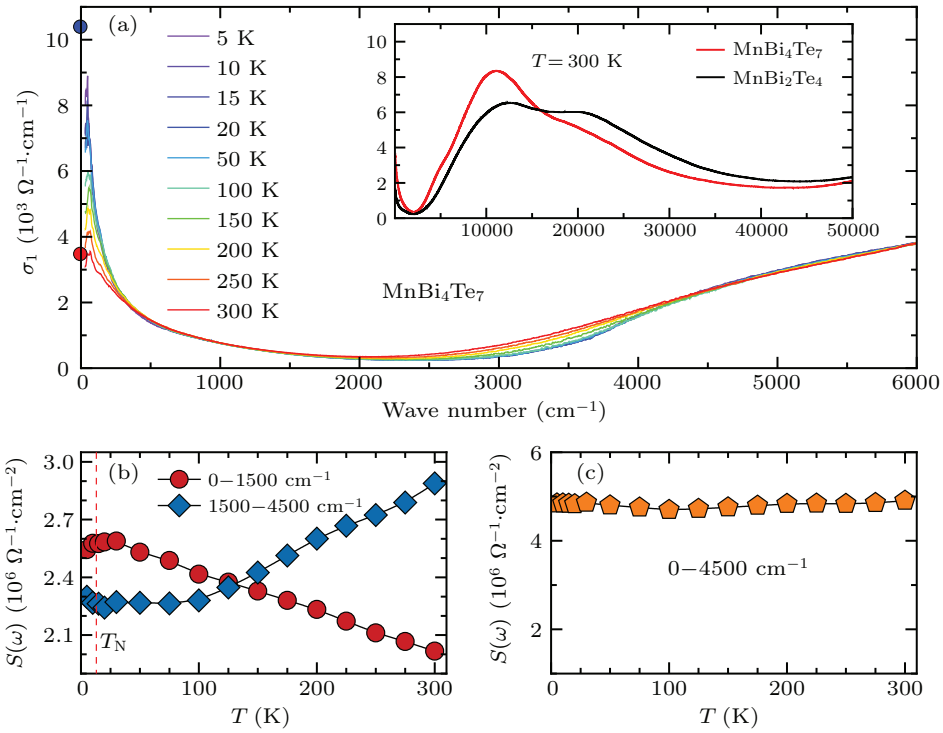


Fig. 2. The real part of the complex optical conductivity and the integrated spectral weight. (a) T dependence of the real part of the complex optical conductivity up to 6000 cm^{-1} for $MnBi_4Te_7$. The symbols on the y axis denote σ_{dc} at 5 K and 300 K from $\rho(T)$ data in the upper inset of Fig. 1(a). Inset: spectrum up to 50000 cm^{-1} at 300 K for $MnBi_4Te_7$ and $MnBi_2Te_4$. (b) T dependence of the integrated spectral weight within 0–1500 cm^{-1} and 1500–4500 cm^{-1}. (c) T dependence of the integrated spectral weight within 0–4500 cm^{-1}.

To have a further analysis of the spectral change in $MnBi_4Te_7$, we calculate the integrated spectral weight (SW), $S(\omega_c) = \int_0^{\omega_c} \sigma_1(\omega)\,d\omega$, where ω_c is the cutoff frequency. Figure 2(b) shows the T evolution of SW within two selected integrating ranges. Firstly, the SW below 1500 cm^{-1} is mainly contributed by the intraband response of free carriers. It gradually increases with decreasing T and exhibits a slight decrease below T_N, aligning with the changes of ω_p^{scr} observed in Fig. 1(b). In contrast, the SW between 1500 cm^{-1} and 4500 cm^{-1} dominated by the interband transitions, decreases upon cooling and shows a small increase below T_N. Moreover, the total SW from 0 to 4500 cm^{-1} keeps nearly a constant under varying T, as is depicted in Fig. 2(c). This suggests a redistribution of spectral weight between the interband and intraband transitions.

Next, we analyze quantitatively the temperature evolution of the free carriers response. A Drude model is introduced to fit the low-frequency $\sigma_1(\omega)$ spectra at all measured temperatures. In this model, the formula writes

$$\sigma_1(\omega) = \frac{2\pi}{Z_0} \sum_j \frac{\omega_{p,j}^2}{\tau_j(\omega^2 + \tau_j^{-2})}, \tag{1}$$

where $Z_0 = 377\ \Omega$ is the vacuum impedance. $\omega_p = \sqrt{4\pi ne^2/m^*}$ is the plasma frequency with n and m^* the concentration and effective mass of charge carries, respectively. And $1/\tau$ describes the scattering rate of carriers.

Figure 3(a) shows an example of the Drude fit for the data at 5 K. The fitting curve is composed of two Drude terms (referred to as Drude 1 and Drude 2) characterized by small and large scattering rates, respectively. Such a fitting method by multiple Drude terms has been widely used in iron-based superconductors[41–43] and the recently discovered kagome superconductors[44] due to the multiband response. The two-Drude fit indicates that $MnBi_4Te_7$ has two types of charge carriers with very different scattering rates. This observation is consistent with the multiband characteristic near the Fermi level (E_F), as supported by the ARPES measurements and band structure calculations in $MnBi_4Te_7$.[34] The fitting parameters, ω_p and $1/\tau$, for the two Drude terms are plotted against temperature in Figs. 3(b) and 3(c), respectively. The narrow Drude term (Drude 1) exhibits strong temperature dependence with an enhanced ω_p and a reduced $1/\tau$ at lower temperature. The broad Drude term (Drude 2) with $\omega_p = 9000$ cm^{-1} and $1/\tau = 850$ cm^{-1} does not change with T, which can also be inferred by the nearly unchange of the Drude tail in T-dependent $\sigma_1(\omega)$, as shown in Fig. 2(a). To further understand the responses of these two types of free carriers, we outlined the band structure of $MnBi_4Te_7$ in inset of Fig. 3(a). This schematic highlights the presence of two distinct conduction bands, denoted as CB1 and CB2. Accordingly, we can attribute the narrow Drude peak to the intraband transitions of CB1, as CB1 is located shallowly below the Fermi level, making it highly sensitive to the thermal effect. In contrast, the broad Drude peak corresponds to intraband transitions of CB2, which is located deeper below the Fermi level and thus is less sensitive to the thermal effect. Additionally, the optical

excitations at higher energy involve transitions across the direct band gap, from the valence band (VB) to the empty states in CB1 and CB2, as indicated by the green arrows.

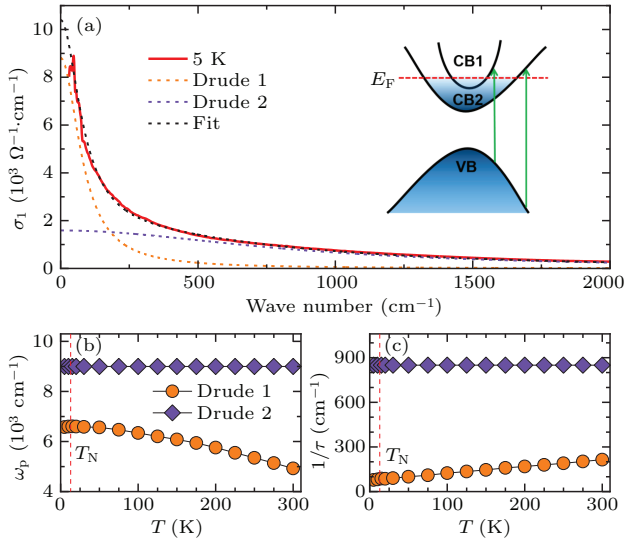


Fig. 3. Drude fitting and the fitting parameters. (a) Drude fitting of $\sigma_1(\omega)$ at 5 K for $MnBi_4Te_7$. Inset: schematic of the band structure. (b) and (c) The T dependence of the two fitting parameters, plasma frequency and the scattering rate, respectively.

Next, we focus on the influence of antiferromagnetic order on the carrier response. Figure 4(a) presents the $\sigma_1(\omega)$ up to 2500 cm^{-1} at three temperatures above and below T_N = 13 K for $MnBi_4Te_7$. Above T_N, $\sigma_1(\omega)$ is nearly unchanged. However, below T_N, we observe a slight decrease in $\sigma_1(\omega)$ below 1000 cm^{-1} and an increase at higher frequencies. These features can be seen clearly in the difference spectra of $\sigma_1(\omega)$ in Fig. 4(b). The anomalous change highlights a transfer of spectral weight and suggests a band reconstruction occurring in the presence of antiferromagnetic order. This band reconstruction is caused by the band folding along k_z and splitting of conduction and valence bands, which lifts the band degeneracy due to the unit cell doubling in the AFM state. Such a band splitting is also seen in recent ARPES study.[22]

Finally, it is worthy to compare the results between $MnBi_4Te_7$ and $MnBi_2Te_4$. In Fig. 4(a), we also plot $\sigma_1(\omega)$ of $MnBi_2Te_4$ at three temperatures above and below T_N = 24 K. In $MnBi_2Te_4$, a clear bump-like feature can be observed around 1100 cm^{-1}, while it is not discernible in $MnBi_4Te_7$. This feature is attributed to the interband transitions between the CB1 and CB2. Here, the featureless response in $MnBi_4Te_7$ suggests a lower joint density of states for such interband transitions. Another different spectral feature is the change of low-frequency $\sigma_1(\omega)$ below T_N, which is enhanced below 500 cm^{-1} in $MnBi_2Te_4$ while it is suppressed in $MnBi_4Te_7$. This result is consistent with the enhancement of Drude SW below T_N for $MnBi_2Te_4$ and the suppression of which for $MnBi_4Te_7$. As outlined in $MnBi_2Te_4$,[40] the anomalous change of Drude SW is related to the shift of center of the splitting conduction bands below T_N with respect to the conduction band above T_N. Thus, the opposite change of Drude weight implies an opposite shift of center of the splitting conduction bands in $MnBi_4Te_7$.

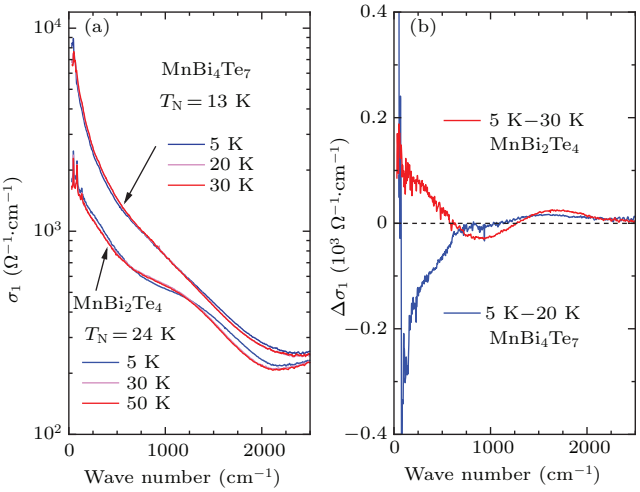


Fig. 4. Anomaly of the optical conductivity across T_N. (a) The $\sigma_1(\omega)$ spectra below 2500 cm^{-1} at selected temperature above and below T_N for $MnBi_4Te_7$ and $MnBi_2Te_4$. (b) The difference plots of $\sigma_1(\omega)$ for $MnBi_4Te_7$ and $MnBi_2Te_4$.

4. Conclusion

In summary, we measured the optical conductivity of the antiferromagnetic topological insulator $MnBi_4Te_7$ over a wide frequency range both above and below T_N. Our optical data reveal the presence of two Drude peaks in the low-frequency region, providing evidence for a multiband free carrier response. Meanwhile, we observe a series of interband transitions originating from valence band states to unoccupied states above the Fermi level, with an onset of interband transitions around 2000 cm^{-1}. With decreasing temperature, we find a transfer of spectral weight from interband transitions to the Drude response. Moreover, the antiferromagnetic transition leads to anomalies in the charge response, affecting the plasma frequency and the transfer of spectral weight below T_N due to the band reconstruction. Our study provides a deep understanding of the interplay between magnetism and electronic properties, and is also helpful in discovering more magnetic topological insulators.

Acknowledgements

Project supported by the the National Natural Science Foundation of China (Grant No. 12274442) and the National Key R&D Program of China (Grant No. 2022YFA1403901).

References

[1] Yu R, Zhang W, Zhang H J, Zhang S C, Dai X and Fang Z 2010 *Science* **329** 61
[2] Xu G, Weng H M, Wang Z J, Dai X and Fang Z 2011 *Phys. Rev. Lett.* **107** 186806

[3] Chang C Z, Zhang J S, Feng X, *et al.* 2013 *Science* **340** 167
[4] Chang C Z, Zhao W W, Kim D Y, Zhang H J, Assaf B A, Heiman D, Zhang S C, Liu C X, Chan M H W and Moodera J S 2015 *Nat. Mater.* **14** 473
[5] Essin A M, Moore J E and Vanderbilt D 2009 *Phys. Rev. Lett.* **102** 146805
[6] Sekine A and Nomura K 2021 *J. Appl. Phys.* **129** 141101
[7] Li R D, Wang J, Qi X L and Zhang S C 2010 *Nat. Phys.* **6** 284
[8] Mong R S K, Essin A M and Moore J E 2010 *Phys. Rev. B* **81** 245209
[9] Xiao D, Jiang J, Shin J H,Wang W B, Wang F, Zhao Y F, Liu C X, Wu W D, Chan M H W, Samarth N and Chang C Z 2018 *Phys. Rev. Lett.* **120** 056801
[10] Otrokov M M, Menshchikova T V, Vergniory M G, Rusinov I P, Vyazovskaya A Y, Koroteev Y M, Bihlmayer G, Ernst A, Echenique P M, Arnau A and Chulkov E V 2017 *2D Mater.* **4** 025082
[11] Gong Y, Guo J W, Li J H, *et al.* 2019 *Chin. Phys. Lett.* **36** 076801
[12] Otrokov M M, Klimovskikh I I, Bentmann H, *et al.* 2019 *Nature* **576** 416
[13] Wu J Z, Liu F C, Sasase M, Ienaga K, Obata Y, Yukawa R, Horiba K, Kumigashira H, Okuma S, Inoshita T and Hosono H 2019 *Sci. Adv.* **5** eaax9989
[14] Yan J Q, Zhang Q, Heitmann T, Huang Z L, Chen K Y, Cheng J G, Wu W D, Vaknin D, Sales B C and McQueeney R J 2019 *Phys. Rev. Materials* **3** 064202
[15] Li H, Liu S S, Liu C, Zhang J S, Xu Y, Yu R, Wu Y, Zhang Y G and Fan S S 2020 *Phys. Chem. Chem. Phys.* **22** 556
[16] Deng Y J, Yu Y J, Shi M Z, Guo Z X, Xu Z H, Wang J, Chen X H and Zhang Y B 2020 *Science* **367** 895
[17] Liu C, Wang Y C, Li H, Wu Y, Li Y X, Li J H, He K, Xu Y, Zhang J S and Wang Y Y 2020 *Nat. Mater.* **19** 522
[18] Ge J, Liu Y Z, Li J H, Li H, Luo T C, Wu Y, Xu Y and Wang J 2020 *Natl. Sci. Rev.* **7** 1280
[19] Chen B, Fei F C, Zhang D Q, *et al.* 2019 *Nat. Commun.* **10** 4469
[20] Chen Y J, Xu L X, Li J H, *et al.* 2019 *Phys. Rev. X* **9** 041040
[21] Hao Y J, Liu P F, Feng Y, *et al.* 2019 *Phys. Rev. X* **9** 041038
[22] Li H, Gao S Y, Duan S F, *et al.* 2019 *Phys. Rev. X* **9** 041039
[23] Swatek P, Wu Y, Wang L L, Lee K, Schrunk B, Yan J Q and Kaminski A 2020 *Phys. Rev. B* **101** 161109
[24] Rienks E D L, Wimmer S, Sánchez-Barriga J, *et al.* 2019 *Nature* **576** 423
[25] Lee S H, Zhu Y L, Wang Y, Miao L X, Pillsbury T, Yi H M, Kempinger S, Hu J, Heikes C A, Quarterman P, Ratcliff W, Borchers J A, Zhang H D, Ke X L, Graf D, Alem N, Chang C Z, Samarth N and Mao Z Q 2019 *Phys. Rev. Research* **1** 012011
[26] Zeugner A, Nietschke F, Wolter A U B, *et al.* 2019 *Chem. Mater.* **31** 2795
[27] Yan J Q, Liu Y H, Parker D S, Wu Y, Aczel A A, Matsuda M, McGuire M A and Sales B C 2020 *Phys. Rev. Materials* **4** 054202
[28] Ding L, Hu C W, Ye F, Feng E X, Ni N and Cao H B 2020 *Phys. Rev. B* **101** 020412
[29] Vidal R C, Zeugner A, Facio J I, *et al.* 2019 *Phys. Rev. X* **9** 041065
[30] Xu L X, Mao Y H, Wang H Y, *et al.* 2020 *Sci. Bull.* **65** 2086
[31] Hu C W, Gordon K N, Liu P F, Liu J Y, Zhou X Q, Hao P P, Narayan D, Emmanouilidou E, Sun H Y, Liu Y T, Brawer H, Ramirez A P, Ding L, Cao H B, Liu Q H, Dessau D and Ni N 2020 *Nat. Commun.* **11** 97
[32] Hu Y, Xu L X, Shi M Z, Luo A Y, Peng S T, Wang Z Y, Ying J J, Wu T, Liu Z K, Zhang C F, Chen Y L, Xu G, Chen X H and He J F 2020 *Phys. Rev. B* **101** 161113
[33] Klimovskikh I I, Otrokov M M, Estyunin D, *et al.* 2020 *npj Quantum Mater.* **5** 54
[34] Wu X F, Li J Y, Ma X M, *et al.* 2020 *Phys. Rev. X* **10** 031013
[35] Vidal R C, Bentmann H, Facio J I, Heider T, Kagerer P, Fornari C I, Peixoto T R F, Figgemeier T, Jung S, Cacho C, Büchner B, van den Brink J, Schneider C M, Plucinski L, Schwier E F, Shimada K, Richter M, Isaeva A and Reinert F 2021 *Phys. Rev. Lett.* **126** 176403
[36] Gordon K N, Sun H Y, Hu C W, Linn A G, Li H X, Liu Y T, Liu P F, Mackey S, Liu Q H, Ni N and Dessau D 2019 arXiv:1910.13943v1 [cond-mat.str-el]
[37] Homes C C, Reedyk M, Cradles D A and Timusk T 1993 *Appl. Opt.* **32** 2976
[38] Roychowdhury S, Singh S, Guin S N, Kumar N, Chakraborty T, Schnelle W, Borrmann H, Shekhar C and Felser C 2021 *Chem. Mater.* **33** 8343
[39] Shi M Z, Lei B, Zhu C S, Ma D H, Cui J H, Sun Z L, Ying J J and Chen X H 2019 *Phys. Rev. B* **100** 155144
[40] Xu B, Zhang Y, Alizade E H, Jahangirli Z A, Lyzwa F, Sheveleva E, Marsik P, Li Y K, Yao Y G, Wang Z W, Shen B, Dai Y M, Kataev V, Otrokov M M, Chulkov E V, Mamedov N T and Bernhard C 2021 *Phys. Rev. B* **103** L121103
[41] Dai Y M, Akrap A, Bud'ko S L, Canfield P C and Homes C C 2016 *Phys. Rev. B* **94** 195142
[42] Yang R, Yin Z P, Wang Y L, Dai Y M, Miao H, Xu B, Qiu X G and Homes C C 2017 *Phys. Rev. B* **96** 201108
[43] Hao J H, Hong W S, Zhou X X, Xiang Y, Dai Y M, Yang H, Li S L, Luo H Q and Wen H H 2022 *Phys. Rev. B* **106** 014523
[44] Zhou X X, Li Y K, Fan X W, Hao J H, Dai Y M, Wang Z W, Yao Y G and Wen H H 2021 *Phys. Rev. B* **104** L041101